Thermal behavior of afghanite, an ABABACAC member of the cancrinite group

PAOLO BALLIRANO[1,2,*] AND FERDINANDO BOSI[1,3]

[1]Dipartimento di Scienze della Terra, Sapienza Università di Roma, P.le Aldo Moro 5, I-00185, Roma, Italy
[2]CNR-IGAG, Istituto di Geologia Ambientale e Geoingegneria, Sede di Roma, Via Bolognola 7, I-00138 Roma, Italy
[3]CNR-IGG Istituto di Geoscienze e Georisorse, Sede di Roma, P.le A. Moro, 5, I-00185 Roma, Italy

ABSTRACT

Thermal behavior of afghanite, $(Na_{15}K_5Ca_{11})_{\Sigma 31}[Si_{24}Al_{24}O_{96}](SO_4)_6Cl_6$, $P31c$, $a = 12.7961(7)$ Å, $c = 21.4094(13)$ Å, an eight-layer member of the cancrinite group, has been investigated by combined electron microprobe analysis, X-ray single-crystal diffraction, and high-temperature X-ray powder diffraction. Non-ambient X-ray powder diffraction data were collected in the 323–1223 K thermal range on a specimen from Case Collina, Latium, Italy. Structural refinement and site assignment based on the bond-valence analysis, performed on room-temperature single-crystal X-ray diffraction data, provided more accurate site allocation of cations than the available model in the literature. The results show that the cancrinite cages alternating with the liottite cages are more compressed along the **c**-axis than the remaining ones. As a result the chlorine atom, located at the center of the cages, is driven off-axis to release the steric strain due to the cage compression. Thermal expansion shows a discontinuity at 448 K for both a and c unit-cell parameters, a feature previously reported for other cancrinite-like minerals. Up to 448 K, the c-parameter expands significantly and more than the a-parameter. A further discontinuity has been detected at 1073 K for the c-parameter. Mean linear and volume thermal expansion coefficients ($\times 10^{-6}$ K^{-1}) in the $323 < T < 448$ K thermal range are $\overline{\alpha_a} = 12.9(4)$, $\overline{\alpha_c} = 17.9(9)$, and $\overline{\alpha_V} = 43.7(18)$. Above this discontinuity temperature, the thermal expansion is reverted becoming greater for the a-parameter. Mean linear and volume thermal expansion coefficients in the $448 < T < 1073$ K thermal range are $\overline{\alpha_c} = 8.22(3)$, $\overline{\alpha_c} = 3.52(4)$, and $\overline{\alpha_V} = 19.68(8)$. In the $1073 < T < 1223$ K thermal range the values are $\overline{\alpha_a} = 6.35(9)$, $\overline{\alpha_c} = 5.02(14)$, and $\overline{\alpha_V} = 17.74(9)$. Afghanite shows a significant microstrain at RT that increases up to ca. 700 K and subsequently decreases as a function of T. Cooling to RT allows a significantly release of ε_0 microstrain, which is coupled with a significant expansion of the c-parameter as compared to the starting RT data. The expansion of the c-parameter has been mainly attributed to the full expansion of the cancrinite cages alternating with the liottite cages. Upon reheating at 1173 K, the microstrain increases back to approximately the same value calculated for the first heating process. Repeated heating-RT-cooling cycles led to the partial afghanite structure disruption and the partial conversion, via an intermediate disordered phase, to haüyne. As repeated heating/cooling cycles did not modify the ε_0 values both at RT and at HT, it can therefore be concluded that the strain release occurs prevalently during the first heating/cooling cycle.

Keywords: Afghanite, cancrinite group, X-ray single-crystal diffraction, high-temperature X-ray powder diffraction, Rietveld method

INTRODUCTION

The relevant structural features of the so-called cancrinite group have been recently reviewed by Bonaccorsi and Merlino (2005). These minerals are built from layers of six-membered rings made of TO_4 (where T is mainly Si and Al) tetrahedra.

The layers are stacked along the **c**-axis following an ABC-based scheme. Among the various members of the group, afghanite represents one of the two known eight-layer phases, the other being alloriite (Chukanov et al. 2007; Rastsvetaeva et al. 2007). It is characterized by an ABABACAC stacking sequence or |1(2)1|1(2)1| following the Zhdanov notation. Afghanite was described as a new mineral species by Bariand et al. (1968) from a specimen from the famous lapislazuli mine

of Sar-e-Sang, Afghanistan. However, Parodi et al. (1996) demonstrated the identity between afghanite and natrodavyne from Mount Vesuvius (Italy), whose description, by the Italian mineralogist Zambonini, dates back to 1910.

A first structure refinement of afghanite was performed in the space group $P6_3mc$ by Merlino and Mellini (1976) considering a disordered Si-Al distribution. Subsequently, Pobedimskaya et al. (1991) performed a new refinement, probably on a sample from the lapislazuli mine in the Lake Baikal region previously described by Ivanov and Sapozhnikov (1975), again in $P6_3mc$, obtaining a good crystallographic R-factor. However, Ballirano et al. (1997) showed the occurrence of a perfect long-range Si-Al order that reduces the symmetry to $P31c$.

Despite the large number of structure refinements at room temperature (RT) of the various cancrinite-group minerals, much less work has been done under non-ambient conditions.

---

* E-mail: paolo.ballirano@uniroma1.it

Moreover, the investigations have been exclusively devoted to simple AB-type minerals. As far as only natural materials are concerned, cancrinite $[(Na,Ca)_{5-6}(CO_3)_{1.4-1.7}][Na_2(H_2O)_2]$ $[Si_6Al_6O_{24}]$ has received a special attention (Ballirano et al. 1995; Hassan 1996a, 1996b; Hassan et al. 2006). Besides, thermal behavior of davyne $[(Na,K)_6(SO_4)_{0.5-1}Cl_{0-1}][Ca_2Cl_2][Si_6Al_6O_{24}]$ and microsommite $[(Na_4K_2(SO_4)][Ca_2Cl_2][Si_6Al_6O_{24}]$ has been reported (Bonaccorsi et al. 1995) as well as that of pitiglianoite $[(Na_4K_2(SO_4)][Na_2(H_2O)_2][Si_6Al_6O_{24}]$ (Bonaccorsi and Merlino 2005).

As no detailed information about the thermal behavior of cancrinite-group minerals showing complex stacking sequences has been reported so far, the aim of this paper is to investigate the dependence of the structure of afghanite from temperature by combining electron microprobe analysis, RT X-ray single-crystal diffraction, and HT parallel-beam laboratory X-ray powder diffraction. The non-ambient structural data obtained from the latter technique have been recently proved to be of very high quality (Ballirano 2011a, 2011b, 2011c) and therefore appear to be perfectly adequate for the proposed task.

EXPERIMENTAL METHODS

Electron microprobe analysis (EMPA)

A sample of afghanite from Case Collina, Latium, Italy, was selected for the present investigation. Prior to undertaking the electron microprobe analysis, a crystal was picked from the hand specimen and embedded in epoxy. After polishing, it was ultrasonically cleaned in deionized water and heated overnight in an oven at 50 °C to eliminate adsorbed H_2O. The analysis was carried out using a Cameca SX50 electron microprobe with the following experimental conditions: 10 s counting time (peak), 5 s counting time (background), beam diameter 10 μm, excitation voltage 15 kV, specimen current 15 nA, wavelength-dispersive spectroscopy. The following standards were used: wollastonite (Si and Ca), corundum (Al), orthoclase (K), jadeite (Na), barite (S), sylvite (Cl), and fluorophlogopite (F). The raw data were corrected online for drift, dead time, and background; matrix correction has been performed with a standard ZAF program. Unit formula was normalized on the basis of 48 (Si+Al). Chemical data and unit formula are reported in Table 1.

X-ray single-crystal structural refinement (SREF)

A fragment of the crystal of afghanite analyzed by EMPA was removed from the resin and used for the single-crystal analysis. Complete intensity data were collected, under room conditions, at the X-ray Diffraction Laboratory of the Dipartimento di Scienze della Terra, Sapienza Università di Roma using a Bruker AXS KAPPA APEX-II diffractometer equipped with CCD area detector $(6.2 \times 6.2 \text{ cm}^2$ active detection area, 512×512 pixels) and a graphite crystal monochromator, using $MoK\alpha$ radiation from a fine-focus sealed X-ray tube. The sample-to-detector distance was 4 cm. A total of 5539 exposures (step = 0.2°, time/step = 20 s) covering a full reciprocal sphere with a high redundancy of about 18

were collected and a completeness of 99.7% was achieved. The orientation of the crystal lattice was determined using more than 800 strong reflections, $I > 100 \sigma(I)$ evenly distributed in reciprocal space, and used for subsequent integration of all recorded intensities. Final unit-cell parameters, $a = 12.7961(7)$, $c = 21.4094(13)$ Å, were refined using Bruker's AXS SAINT program on reflections with $I > 10$ $\sigma(I)$ in the range $5° < 2\theta < 65°$. The intensity data were processed and corrected for Lorentz, polarization, and background effects with the APEX2 software program of Bruker AXS. The data were corrected for absorption using multi-scan method (SADABS). The absorption correction led to a significant improvement in R_{int}.

The refinement was carried out using SHELXL-97 (Sheldrick 2008) with the framework fractional coordinates of Ballirano et al. (1997) as starting point. The structure was completed by cycles of difference-Fourier syntheses. Details on the data collection and the structure refinement are reported in Table 2. Structural data at RT and at selected T have been submitted as CIF[1] files.

High-temperature X-ray powder diffraction (HT-XRPD)

A few crystals of afghanite were selected, removed from the hand specimen, and crushed under ethanol in an agate mortar. The powder was loaded and packed in 0.5 mm diameter quartz-glass capillary that was fixed to a 1.0 mm diameter Al_2O_3 tube by means of a high-purity alumina ceramic (Resbond 989). The capillary/tube assembly was subsequently aligned onto a standard goniometer head and diffraction data were collected on a parallel-beam Bruker AXS D8 Advance, operating in transmission in θ-θ geometry. The instrument is fitted with a PSD VÅNTEC-1 detector set to a 6 °2θ aperture and with a prototype of capillary heating chamber (Ballirano and Melis 2007).

Non-ambient data were collected in the 6–140 °2θ angular range, with 4 s of counting time, in the 323–1223 K thermal range with temperature steps of 25 K. A magnified view of the full data set is reported in Figure 1.

The capillary was subsequently slowly cooled down to RT and a measurement under the same experimental conditions was carried out.

Moreover, three kinetics experiments were carried out on the thermally treated capillary. The first one was performed isothermally at 1173 K. The capillary was then cooled back to RT and subsequently reheated at 1198 K to collect the second data set. Finally, a further cooling/heating cycle at 1198 K was performed.

Diffraction data were evaluated by the Rietveld method with the GSAS suite of programs (Larson and Von Dreele 2000) coupled with the EXPGUI graphical user interface (Toby 2001).

A structure refined at a given temperature was used as input for the subsequent temperature. Peak shapes were modeled by a TCH pseudo-Voigt function modified to incorporate asymmetry (Thompson et al. 1987; Finger et al. 1994). Refined profile variables included, along with the sample displacement from the

TABLE 1. Chemical data and formula unit, calculated on the basis of 48 (Si+Al) for afghanite

	(a)	(b)		(a)	(b)
SiO_2	31.58	31.05	Si	24.29	24.00
Al_2O_3	26.15	26.34	Al	23.71	24.00
			$\Sigma_{(Si+Al)}$	48	48
CaO	12.94	13.35	Ca	10.67	11.06
Na_2O	11.45	10.14	Na	17.08	15.20
K_2O	3.44	5.05	K	3.38	4.98
			$\Sigma_{cations}$	31.13	31.24
SO_3	10.84	10.39	SO_4	6.26	6.03
Cl	4.39	4.57	Cl	5.72	5.99
F	0.05	0.02	F	0.12	0.05
	100.84	100.91			
O=Cl,F	−1.01	−1.04	O	95.86	96.10
Total	99.83	99.87			

Note: (a) Reference chemical data of Ballirano et al. (1997); (b) present work.

TABLE 2. Crystal data and structure refinement details for afghanite

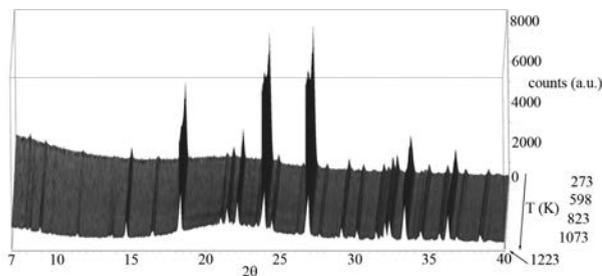| Ideal chemical formula	$(Na_{15}K_5Ca_{11})_{\Sigma=32}[Si_{24}Al_{24}O_{96}](SO_4)_6Cl_6$
Wavelength (Å)	0.71073
Space group	$P31c$
Cell parameters (Å)	$a = 12.7961(7)$
	$c = 21.4094(13)$
Volume (Å³)	3035.92(2)
Crystal size (mm)	$0.30 \times 0.30 \times 0.35$
2θ max (°)	65.33
Index ranges	$−11 \leq h \leq 19$
	$−19 \leq k \leq 12$
	$−32 \leq l \leq 30$
Reflections collected	72135
Independent reflections	7339 [$R_{int} = 0.0290$]
Completeness (%)	99.7
Refinement method	Full-matrix least-squares on F^2
Data/parameters	7339/352
Goodness-of-fit on F^2	1.080
Final R indices [$I > 2\sigma(I)$]	$R1 = 0.0383$
	$wR2 = 10.00$
R indices (all data)	$R1 = 0.0430$
	$wR2 = 10.00$
Flack x parameter	0.07(5)
Largest diff. peak and hole (e·Å⁻³)	−1.66 and 0.62

FIGURE 1. Magnified 3D view (7–40 °2θ) of the full data set of the 323–1223 K heating cycle of afghanite.

goniometer focusing circle, the GV tan θ-dependent Gaussian parameters, and the LX 1/cos θ-dependent Lorentzian parameter. The peak cut-off was set to 0.1% of the peak maximum and the background was fitted with a 36 terms Chebyshev polynomial of the first kind. Such a large number of parameters were required to properly model the contribution of the capillary and the rapidly decaying incident beam contribution at low 2θ values. A total of 108 restraints on tetrahedral bond distances [Si-O: 1.610(14); Al-O: 1.730(14); S-O: 1.46(2)] and O-T-O angles, expressed as pseudobonds, were imposed. Statistical associated weight was set to 4. Restraints contribution to χ^2 never exceeded 5% indicating a proper weighting scheme. Isotropic displacement parameters were refined constraining those of similar sites to be equal and allowing the refinement of the occupancy of the various cations at the M sites. As in the case of the single-crystal structure refinement, the potassium scattering power was used to model the M sites. An absorption measurement has been carried out collecting the transmitted beam through the sample $I_t(E)$ and the incident primary beam $I_0(E)$, both in direct transmission. The derived μ_{eff} was kept fixed during the refinements.

An evaluation of texture was carried out by means of a generalized spherical-harmonic (Von Dreele 1997) description up to the spherical harmonic order of six, including 6 refinable l,m,n terms: 2,0,0; 4,0,0; 4,0,3; 6,0,0; 6,0,3; 6,0,6. The choice of the number of terms to be used has been performed according to Ballirano (2003). As expected for a capillary mount, an almost complete absence of preferred orientation was observed as a result of calculated texture indices J close to one. During the final refinement cycles, the coefficients of the various l,m,n terms were kept fixed to the corresponding mean values, as calculated from the various diffraction patterns leading to an average J of 1.0548. Similarly, M-site occupancies were found to be extremely constant throughout the refinements, the only exception being the difficulty to independently refine the disordered M4 and M4a sites. Therefore, during the final refinement cycles a single M4 site was used and the occupancies of the various sites were fixed to the corresponding mean values (M1 = 0.796, M2 = 0.729, M3 = 0.631, M4+M4a = 0.817). Individual site

occupancies are reasonably close to those determined from SREF. The total number of electrons assigned to the M sites from HT-XRPD is of 339(9) e$^-$ as compared to 336(6) e$^-$ from SREF (see below) and 323 from EMPA. An example of Rietveld plots at 823 K is shown in Figure 2; experimental details and miscellaneous data of the refinements are reported in Table 3.

A further set of refinements was carried out using TOPAS v. 4.2 (Bruker AXS 2009). This program implements the fundamental parameters approach (FPA) (Cheary and Coelho 1992). FPA is a convolution approach in which the peak shape is synthesized from a priori known features of the diffractometer (i.e., the emission profile of the source, the width of the slits, and the angle of divergence of the incident beam) and the microstructural features of the specimen. This approach is thought to improve the stability and the quality of the refinement, especially with respect to the extraction of microstructural parameters. At each T, structural data obtained from the first set of Rietveld refinements were used as input and were kept fixed, to refine exclusively the microstructural parameters.

DISCUSSION

Chemical data

The chemical composition of the present afghanite is quite similar to that of the sample coming from Pitigliano (Tuscany), which was chemically and structurally characterized by Ballirano et al. (1996a, 1997). However, with respect to this latter sample, the present afghanite shows an increased K and Ca content by about 2 and 11 atoms per formula unit (apfu), respectively, and an F content very close to the detection limit. The sum of Na, K, and Ca cations per formula unit (31.24) is slightly smaller than those expected (32 apfu). However, as pointed out by Ballirano et al. (1997), more than 10 apfu of Ca induces a reduction of the total number of cations from the maximum possible content of 32. Consequently, the ideal structural formula of the analyzed afghanite may be approximated as $(Na_{15}K_5Ca_{11})_{\Sigma 31}$ $[Si_{24}Al_{24}O_{96}](SO_4)_6Cl_6$.

RT crystal structure

The RT SREF confirms the general features depicted by Ballirano et al. (1997) and provides an improved precision on bond distances and angles, and a few details arising from a slightly different chemistry and an improved data resolution. Moreover, more detailed information on the occupation of the cation sites was obtained. Atomic fractional coordinates, site occupancy, and equivalent isotropic displacement parameters are reported in Table 4, anisotropic displacement parameters in Table 5, and selected bond distances and angles in Table 6.
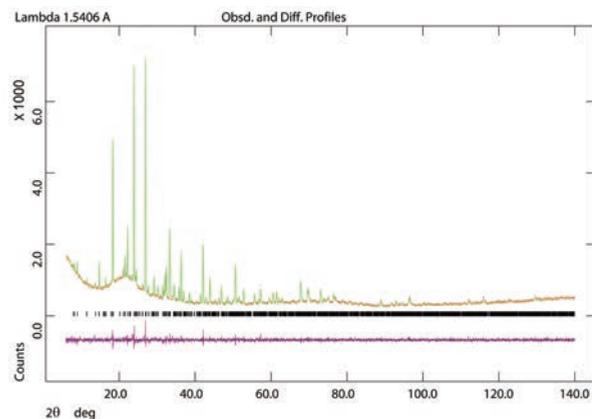

FIGURE 2. Fitted X-ray diffraction pattern obtained at 823 K. The lower curve represents the difference between observed and calculated profiles. Vertical marks refer to the position of calculated Bragg reflections. (Color online.)

TABLE 3. Miscellaneous data of the non-ambient condition Rietveld refinements

Instrument	Bruker-AXS D8 Advance
X-ray tube	Cu operating at 40 kV and 40 mA
Incident beam optics	60 mm multilayer (Göbel) X-ray mirror
Sample mount	Rotating capillary (60 r/min)
Soller slits	2: 2.3° incident beam; radial diffracted beam
Divergence slit	0.6 mm
Detector	PSD VÅNTEC-1
Data range (°2θ)	7–140
Step size (°2θ)	0.022
Counting time (s)	4
wR_p (%)	4.97–5.66
R_p (%)	3.77–4.33
R_{F2} (%)	8.23–11.17
χ^2	1.479–1.621
DWd	1.388–1.535
Contribution of restraints to χ^2 (%)	1.99–4.94

Note: Disagreement indices as defined in Young (1993).

Framework

In line with the values of mean bond lengths <Si-O> = 1.610 Å and <Al-O> = 1.729 Å, it is confirmed that Si and Al are fully ordered among the different tetrahedral sites building up the framework. These values show, apart from an <Al-O> distance slightly larger, a smaller distortion than those reported by Ballirano et al. (1997). The <Si-O>/<Al-O> ratio has a value of 0.931 identical to that observed in liottite (Ballirano et al. 1996b) and slightly smaller than 0.936 reported in the previous afghanite-structure refinement (Ballirano et al. 1997). The framework consists of columns of cancrinite or ε cages ([$4^6 6^5$] polyhedra following the IUPAC nomenclature, McCusker et al. 2001) stacked along the threefold axis located at 0, 0, z, and regularly alternating liottite ([$4^6 6^{17}$] polyhedra) and cancrinite cages piled along the threefold axes located at 2/3, 1/3, z and 1/3, 2/3, z. In total, six cancrinite and two liottite cages occur in the afghanite structure. Only three T-O-T angles, Si3-O5-Al3,

TABLE 4. Atomic coordinates (x 10⁴), site multiplicity, site occupancy, and equivalent isotropic displacement parameters (Å² x 10⁴) for afghanite at room T

Site	x	y	z	Multiplicity	Occupancy	U_{eq}
Si1	7476(1)	7469(1)	4955(1)	1	1	75(1)
Si2	766(1)	6618(1)	8695(1)	1	1	79(3)
Si3	7488(1)	7443(1)	7449(1)	1	1	67(1)
Si4	768(1)	6615(1)	6218(1)	1	1	68(2)
Al1	−14(2)	7409(1)	9958(1)	1	1	78(2)
Al2	5963(1)	6757(1)	8687(1)	1	1	80(3)
Al3	7382(1)	9958(1)	7453(1)	1	1	73(2)
Al4	5964(1)	6757(1)	6223(1)	1	1	77(3)
O1	−95(3)	6612(3)	6764(2)	1	1	154(7)
O2	6837(4)	6716(4)	6826(2)	1	1	191(8)
O3	41(3)	6518(3)	8054(2)	1	1	157(7)
O4	6663(4)	6635(4)	8028(2)	1	1	207(8)
O5	7688(1)	8783(2)	7464(1)	1	1	149(3)
O6	−5(4)	6650(3)	9277(2)	1	1	167(7)
O7	6776(4)	6762(4)	4336(2)	1	1	197(8)
O8	138(4)	6564(3)	5544(2)	1	1	140(6)
O9	6593(4)	6685(4)	5520(2)	1	1	213(8)
O10	8755(4)	7595(2)	5039(1)	1	1	222(5)
O11	7749(2)	8851(4)	4962(1)	1	1	185(4)
O12	8819(2)	7636(2)	7518(1)	1	1	182(3)
O13	912(2)	5438(4)	6271(1)	1	1	232(5)
O14	881(2)	5423(4)	8776(1)	1	1	211(4)
O15	2131(4)	7730(4)	6273(1)	1	1	184(5)
O16	2138(4)	7709(4)	8683(1)	1	1	181(5)
Ca1	0	0	5021(1)	1/3	1	140(1)
Ca2	0	0	7516(1)	1/3	1	128(1)
Ca3	3333	6667	6324(1)	1/3	1	204(2)
Ca4	3333	6667	8780(1)	1/3	1	285(3)
Cl1	0	0	6261(1)	1/3	1	676(7)
Cl2	0	0	8763(1)	1/3	1	660(7)
Cl3	3000(15)	6436(17)	7532(1)	1	1/3	712(34)
M1	5606(1)	7815(2)	3628(1)	1	0.791(4)	358(3)
M2	50(1)	4982(1)	4905(1)	1	0.796(3)	332(2)
M3	5191(2)	4883(2)	7407(1)	1	0.573(3)	394(4)
M4	7774(8)	5553(5)	6268(4)	1	0.486(23)	541(16)
M4a	7910(12)	5768(15)	6178(4)	1	0.304(23)	596(27)
S1	6667	3333	7450(1)	1/3	1	421(3)
S2	3333	6667	4651(1)	1/3	1	285(3)
S3	3333	6667	322(1)	1/3	1	694(8)
OS1a	4097(13)	7754(12)	2626(6)	1	1/3	629(39)
OS1b	4461(15)	7585(15)	2192(9)	1	1/3	835(51)
OS1c	4220(14)	6776(15)	2941(8)	1	1/3	756(44)
OS1d	3742(15)	7769(11)	1983(6)	1	1/3	589(32)
OS2a	3333	6667	5303(4)	1/3	1	1571(61)
OS2b	2098(4)	5990(7)	4411(2)	1	1	716(13)
OS3a	2320(15)	5780(16)	714(8)	1	1/3	769(49)
OS3b	2140(13)	6200(16)	443(6)	1	1/3	541(32)
OS3c	2779(13)	6387(38)	9771(8)	1	1/3	984(53)
OS3d	2064(20)	5980(47)	-39(13)	1	1/3	1390(77)

Note: U_{eq} is defined as one third of the trace of the orthogonalized U_{ij} tensor.

TABLE 5. Anisotropic displacement parameters (Å² x 10³) for afghanite at room T

	U_{11}	U_{22}	U_{33}	U_{23}	U_{13}	U_{12}
Si1	57(4)	71(5)	94(4)	−12(5)	1(5)	30(2)
Si2	93(5)	73(5)	67(5)	0(4)	1(4)	40(4)
Si3	62(3)	79(5)	76(4)	−9(5)	−6(5)	39(2)
Si4	90(5)	64(5)	55(5)	2(4)	8(4)	43(4)
Al1	72(3)	76(5)	65(4)	11(6)	8(2)	21(5)
Al2	77(3)	82(5)	80(7)	2(5)	1(4)	40(4)
Al3	74(3)	74(3)	59(4)	3(6)	6(6)	29(2)
Al4	66(5)	56(5)	99(6)	1(5)	−2(4)	23(4)
O1	163(12)	140(13)	86(15)	−49(11)	−9(10)	22(10)
O2	287(16)	183(15)	138(15)	−93(11)	−159(12)	145(13)
O3	215(14)	149(13)	103(16)	1(10)	−31(10)	88(10)
O4	236(15)	123(13)	230(19)	11(12)	109(13)	65(11)
O5	172(7)	91(8)	207(7)	−38(15)	3(9)	82(7)
O6	212(15)	142(13)	98(16)	−2(11)	31(11)	52(11)
O7	184(16)	280(15)	115(14)	−131(12)	−84(12)	106(14)
O8	210(13)	178(13)	66(14)	−11(10)	−34(10)	122(10)
O9	258(15)	128(13)	202(18)	32(12)	110(13)	60(12)
O10	106(14)	306(11)	297(10)	−102(9)	−17(13)	135(13)
O11	213(10)	63(13)	256(10)	−11(12)	23(7)	52(13)
O12	125(10)	224(8)	253(10)	−43(8)	−50(14)	128(9)
O13	260(11)	141(15)	367(12)	13(15)	12(8)	154(14)
O14	290(11)	110(14)	289(10)	14(13)	19(8)	141(14)
O15	116(14)	117(14)	291(11)	14(12)	−4(12)	38(9)
O16	103(14)	108(14)	269(11)	28(12)	−11(12)	6(10)
Ca1	131(2)	131(2)	157(4)	0	0	65(1)
Ca2	116(2)	116(2)	153(4)	0	0	58(1)
Ca3	141(2)	141(2)	330(6)	0	0	70(1)
Ca4	166(3)	166(3)	524(8)	0	0	83(1)
Cl1	946(12)	946(12)	134(6)	0	0	473(6)
Cl2	918(11)	918(11)	141(6)	0	0	459(6)
Cl3	963(85)	721(56)	245(12)	−23(32)	188(36)	265(47)
M1	470(7)	265(9)	413(6)	28(8)	96(4)	239(9)
M2	569(6)	236(7)	295(4)	−48(7)	−120(3)	281(7)
M3	295(8)	335(8)	352(7)	23(12)	3(12)	8(4)
M4	301(19)	380(23)	962(44)	−10(15)	−61(29)	186(18)
M4a	416(44)	1347(83)	300(27)	67(30)	83(25)	647(55)
S1	425(4)	425(4)	414(7)	0	0	213(2)
S2	310(4)	310(4)	234(6)	0	0	155(2)
S3	878(13)	878(13)	324(10)	0	0	439(6)
OS2a	2253(97)	2253(97)	206(3)	0	0	1127(61)
OS2b	306(16)	592(33)	1198(35)	−134(39)	−220(19)	185(25)

Note: The anisotropic displacement factor exponent takes the form: $-2\pi^2[h^2 a^{*2} U_{11} + ... + 2hka^* b^* U_{12}]$.

Si1-O11-Al1, and Si4-O13-Al4, show differences exceeding 2° with respect to reference data. In particular, Si1-O11-Al1 has been refined to 156.5(1)° as compared to 160.1(3)° recalculated from the original data of Ballirano et al. (1997).

Cancrinite cages

Reference data report geometrical differences between the cancrinite cages forming the uninterrupted chain and those regularly alternating with the liottite cages. In fact, those pertaining to the columnar stacking host a regular ...Ca1-Cl1-Ca2-Cl2... chain (Fig. 3). On the contrary, the ε cages sharing both bases with liottite cages were characterized by a partial Cl3 → F substitution leading to an off-axis displacement of F and a shifting of the two Ca3a and Ca4a atoms toward the center of the cage (Fig. 4). Such coupled Cl → F substitution and Ca atoms shift also occurs in liottite (Ballirano et al. 1996b). The Cl thermal ellipsoids have been reported to be consistently flattened in both structure and this has been interpreted in terms of a small off-axis displacement of the Cl atoms that was found impossible to model using a static disorder.

In the case of the present afghanite, characterized by the nearly complete absence of F, it is the Cl3 atom that is signifi-

TABLE 6. Selected bond distances (Å) and angles (°) for afghanite at room T

Si1-O10	1.572(5)	Si2-O6	1.603(4)	Si3-O2	1.601(4)	Si4-O1	1.607(4)
Si1-O7	1.603(4)	Si2-O16	1.606(5)	Si3-O5	1.602(2)	Si4-O13	1.611(5)
Si1-O9	1.616(5)	Si2-O14	1.618(5)	Si3-O12	1.602(3)	Si4-O15	1.614(5)
Si1-O11	1.622(5)	-O3	1.627(5)	Si3-O4	1.621(5)	Si4-O8	1.637(4)
<Si1-O>	*1.603(22)*	*<Si2-O>*	*1.613(11)*	*<Si3-O>*	*1.606(10)*	*<Si4-O>*	*1.617(13)*
Al1-O11	1.712(5)	Al2-O7	1.719(4)	Al3-O12	1.723(3)	Al4-O15	1.708(5)
Al1-O8	1.728(4)	Al2-O4	1.720(5)	Al3-O3	1.731(5)	Al4-O13	1.726(5)
Al1-O10	1.741(5)	Al2-O16	1.721(5)	Al3-O5	1.733(2)	Al4-O2	1.726(5)
Al1-O6	1.754(4)	Al2-O14	1.730(5)	Al3-O1	1.761(4)	Al4-O9	1.730(5)
<Al1-O>	*1.734(18)*	*<Al2-O>*	*1.723(5)*	*<Al3-O>*	*1.737(17)*	*<Al4-O>*	*1.723(10)*
Ca1-O11 ×3	2.498(2)	Ca2-O5 ×3	2.566(2)	Ca3-OS2a	2.185(8)	Ca4-OS3c	2.209(17)
Ca1-Cl1	2.656(2)	Ca2-O12 ×3	2.620(2)	Ca3-O15 ×3	2.514(2)	Ca4-O16 ×3	2.490(2)
Ca1-O10 ×3	2.666(2)	Ca2-Cl2	2.669(2)	Ca3-Cl3	2.614(4)	Ca4-Cl3	2.698(3)
Ca1-Cl2	2.694(2)	Ca2-Cl1	2.686(2)	Ca3-O13 ×3	2.686(2)	Ca4-O13 ×3	2.718(2)
M1-OS1c	2.173(16)	M2-OS3d	2.35(2)	M3-OS1a	2.222(13)	M4-OS3a	2.029(19)
M1-OS2b	2.701(8)	M2-O8	2.399(4)	M3-OS1d	2.320(12)	M4-OS1b	2.36(2)
M1-O4	2.738(5)	M2-O9	2.430(5)	M3-O3	2.434(4)	M4-OS1d	2.476(18)
M1-O3	2.768(5)	M2-OS2b	2.503(5)	M3-O4	2.474(5)	M4-O1	2.589(9)
M1-O6	2.787(5)	M2-O7	2.523(5)	M3-OS1b	2.545(17)	M4-O2	2.620(9)
M1-OS2b	2.806(8)	M2-O6	2.553(4)	M3-O2	2.559(5)	M4-OS3b	2.644(18)
M1-OS1a	2.861(13)	M2-O14	2.628(2)	M3-O1	2.581(5)	M4-OS1d	2.775(18)
M1-O7	2.893(2)	M2-OS3b	2.695(15)	M3-O1	2.784(3)	M4-OS3a	2.876(18)
M4a-OS3a	2.12(2)	S1-OS1a ×3	1.294(13)	M3-OS1c	2.803(16)	M4-OS3b	2.897(18)
M4a-O1	2.549(12)	S1-OS1b ×3	1.439(17)			M4-O9	3.023(10)
M4a-O2	2.635(12)	S1-OS1c ×3	1.502(16)			M4-O8	3.052(10)
M4a-OS1b	2.64(2)	S1-OS1d ×3	1.589(12)	Si4-O1-Al3	137.9(2)	Si1-O9-Al4	144.8(3)
M4a-OS3b	2.67(2)	*<S1-O>*	*1.46*	Si3-O2-Al4	139.6(3)	Si1-O10-Al1	163.19(17)
M4a-OS1d	2.77(2)	S2-O2a	1.396(8)	Si2-O3-Al3	139.9(2)	Si1-O11-Al1	156.52(15)
M4a-O8	2.847(13)	S2-O2b ×3	1.465(4)	Si3-O4-Al2	140.5(3)	Si3-O12-Al3	161.54(13)
M4a-O9	2.861(14)	*<S2-O>*	*1.45*	Si3-O5-Al3	160.65(11)	Si4-O13-Al4	167.46(18)
M4a-OS3b	2.97(2)	S3-OS3a ×3	1.330(16)	Si2-O6-Al1	146.5(3)	Si2-O14-Al2	165.29(16)
M4a-OS3a	2.99(2)	S3-OS3b ×3	1.358(15)	Si1-O7-Al2	147.4(3)	Si4-O15-Al4	155.15(17)
M4a-OS1d	3.04(2)	S3-OS3c ×3	1.484(18)	S14-O8-Al1	144.5(3)	Si2-O16-Al2	154.15(17)
		S3-OS3d ×3	1.61(2)				
		<S3-O>	*1.45*				

cantly displaced off-axis to release the steric strain due to the cage compression (see below) The Cl3 thermal ellipsoid has a magnitude and shape similar to those of Cl1 and Cl2, which are located alternating along the **c**-axis. As both Ca3 and Ca4 have a thermal ellipsoid slightly elongated along the **c**-axis, it is possible to relate it to a dynamic instead of a static disorder. No indications of Cl → H_2O substitution were observed.

A more detailed analysis of the geometry of the various cancrinite cages clearly indicates that the Cl3-centered cage is the smallest one. In fact the base-to-base height of the cage is of 5.290 Å compared to 5.340 and 5.365 Å of those centered by Cl1 and Cl2, respectively. Such values have been calculated as the average between the vertical distances between pairs of tetrahedral T-cations (Si-Si and Al-Al) pertaining to the bases of the cages. The value of 5.365 Å is comparable to that found in davyne, microsommite, and quadridavyne, i.e., fully expanded Cl end-members of the AB cancrinite-type minerals (Ballirano 1994). Therefore, the relevant off-axis displacement of Cl3 is strictly related to the compression along the **c**-axis of the corresponding cage. Such compression is obtained by a reduction of the corresponding T-O-T angles involving the T-sites bridging adjacent layers [Si4-O1-Al3 = 139.9(2)°, Si3-O2-Al4 = 139.6(3)°, Si2-O3-Al3 = 139.9(2)°, and S13-O4-Al2 = 140.5(3)°].

Another interesting point concerns the different coordination environment of Ca1, Ca2, Ca3, and Ca4. In the case of Ca1 and Ca2, the cation is eightfold-coordinated to six framework oxygen atoms and two chlorine anions. The resulting coordination

polyhedron is quite regular with bond distances in the 2.50–2.70 Å range, a little bit more spread out than reference data (Ballirano et al. 1997). Instead, both Ca3 and Ca4 are linked to six framework oxygen atoms, one clorine, and a further, close (ca. 2.20 Å) oxygen atom pertaining to a neighboring sulfate group, leading to a significantly distorted coordination polyhedron.

Liottite cages and cation sites partition

The liottite cages are ubiquitously found in long-sequence members of the cancrinite-sodalite supergroup (Bonaccorsi et al. 2012). They host three sulfate groups, five triplets of cations distributed onto five planes, and a calcium atom at the center of the two bases. The main differences among the various liottite cages are related to the degree of disorder of the hosts. In the case of both afghanite samples, one of the three sulfate groups (S2) consists of a triple of oxygen atoms (OS2b) lying in a plane normal to the **c**-axis and an apical oxygen OS2a located along the **c**-axis (Fig. 5). It is worth noting that OS2a (bonded to Ca3), despite of being located in-axis, shows a flattened thermal ellipsoid, similar to the various chlorine atoms. The same apply to the OS2b basal atoms. Attempts to model such behavior by static disorder models failed, suggesting the occurrence of a dynamic disorder.

The remaining S1 and S3 centered sulfate groups show a 120° rotational disorder along the threefold axis. The coordination of the two sulfate groups is similar as the oxygen atoms occur at four different positions with 1/3 occupancy.

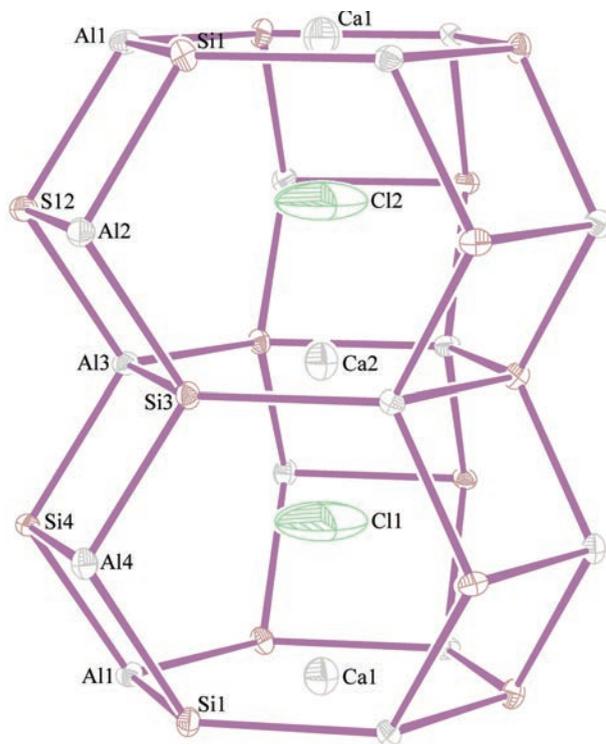A triplet of cations is located approximately at the same z

FIGURE 3. Column of cancrinite cages stacked along the threefold axis located at 0, 0, *z*. Framework oxygen atoms not plotted. (Color online.)
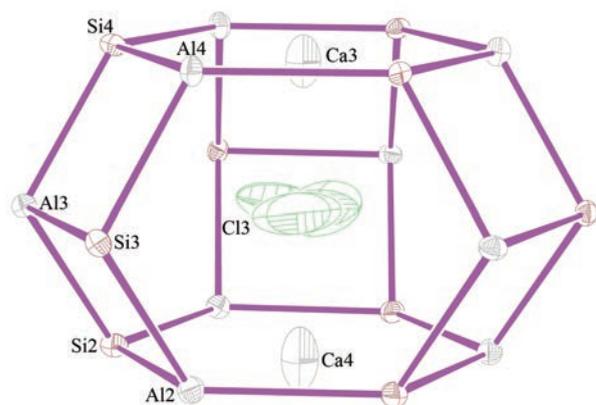

FIGURE 4. Cancrinite cage sharing its bases with neighboring liottite cages. Framework oxygen atoms not plotted. (Color online.)

FIGURE 5. Liottite cage. For clarity, oxygen atoms of both sulfate groups and framework have been not plotted. (Color online.)

elevation of each sulfur atom and a further triplet is located midway. In the case of the present sample of afghanite, only the M4 site is split differently from reference data that reported additional splitting for the M1 site (Ballirano et al. 1997) or for M1, M2, and M3 (Pobedimskaya et al. 1991). However, the latter example of extended disorder may arise because of higher symmetry ($P6_3mc$) proposed by the authors.

Bond-valence analysis (empirical parameters from Brese and O'Keeffe 1991) provided important clues for a meaningful cation site partition (Table 7). Ballirano et al. (1997) derived the cation site populations from the site-scattering values as-
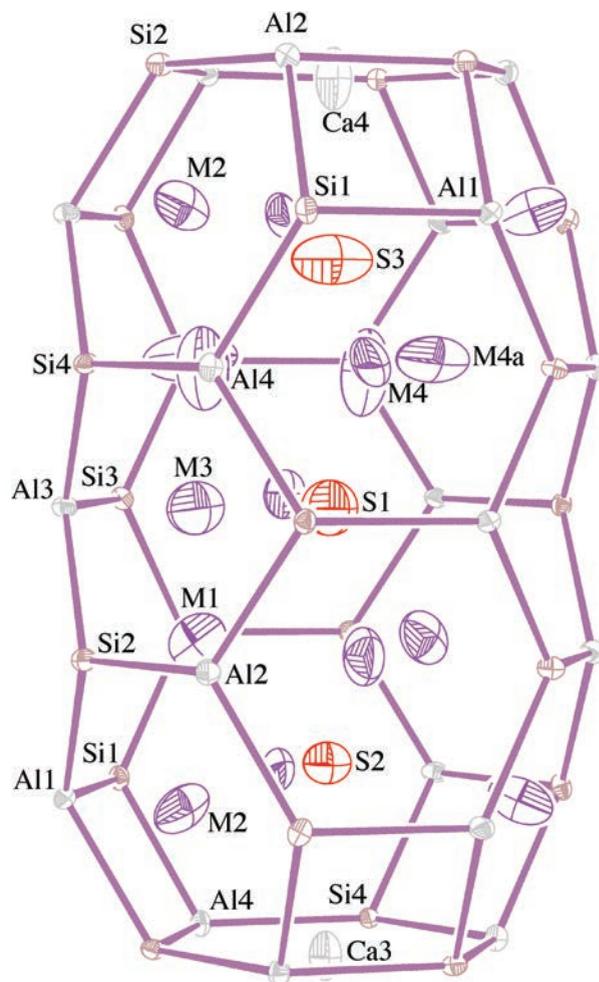
suming a full occupancy for the sum of split sites. Therefore, no attempt to discriminate between K$^+$ and Ca^{2+} was performed. In the present work, exploiting an improved precision on the observed bond distances we have attempted a more detailed site allocation of cations. In fact, M1 can be potentially filled either by K$^+$ or Na$^+$ because Ca^{2+} cannot reach a sum of 2 valence units (v.u.). M2 and M3 do not accommodate K$^+$ as both sites receive bond-valence sums largely exceeding 1 v.u. No constraints were found for the occupancy of M4 and M4a sites.

Due to the lack of constraints on the distribution of vacancies on the cation sites, our proposed site populations could be subjected to significant amounts of uncertainty. In this regard, however, various models were tested and the most reasonable one, in terms of site-scattering values and bond-valence sums, suggested an even distribution of 1 vacancy pfu onto the split M4+M4a sites. The result of this approach showed (Table 8) an excellent agreement between calculated and observed site-scattering values for the M1, M2, and M3 sites, whereas M4a and M4 deviated by about 3 and 11 e$^-$ from the observed values. The large discrepancy obtained for M4 could be related to the

TABLE 7. Bond valence analysis for the cation sites of afghanite at room T

	M1				M2				M3		
	K	Na	Ca		K	Na	Ca		K	Na	Ca
OS1c	0.890	0.365	0.573	OS3d	0.559	0.229	0.359	OS1a	0.780	0.320	0.502
OS2b	**0.214**	**0.088**	**0.138**	O8	**0.483**	**0.198**	**0.311**	OS1d	0.598	0.245	0.385
O4	**0.193**	**0.079**	**0.125**	O9	**0.445**	**0.182**	**0.286**	O3	**0.440**	**0.180**	**0.283**
O3	**0.178**	**0.073**	**0.115**	OS2b	**0.365**	**0.150**	**0.235**	O4	**0.395**	**0.162**	**0.254**
O6	**0.169**	**0.069**	**0.109**	O7	**0.346**	**0.142**	**0.223**	OS1b	0.326	0.134	0.210
OS2b	**0.161**	**0.066**	**0.104**	O6	**0.319**	**0.131**	**0.205**	O2	**0.314**	**0.129**	**0.202**
OS1a	0.139	0.057	0.089	O14	**0.260**	**0.107**	**0.169**	O1	**0.296**	**0.121**	**0.190**
O7	**0.121**	**0.052**	**0.082**	OS3b	0.217	0.089	0.140	O13	**0.171**	**0.070**	**0.110**
								OS1c	0.162	0.067	0.104
Total fixed	**1.036**	**0.427**	0.673		**2.218**	**0.910**	**1.429**		**1.616**	**0.662**	**1.039**
Population	*	*				*	*			*	*

	M4				M4a		
	K	Na	Ca		K	Na	Ca
OS3a	1.314	0.539	0.846	OS3a	1.016	0.417	0.654
OS1b	0.533	0.218	0.343	O1	**0.322**	**0.132**	**0.207**
OS1d	0.393	0.161	0.253	O2	**0.255**	**0.105**	**0.164**
O1	**0.289**	**0.119**	**0.186**	OS1b	0.251	0.103	0.161
O2	**0.266**	**0.109**	**0.171**	OS3b	0.233	0.096	0.150
OS3b	0.249	0.102	0.161	OS1d	0.176	0.072	0.113
OS1d	0.175	0.072	0.113	O8	**0.144**	**0.059**	**0.093**
OS3a	0.133	0.055	0.086	O9	**0.139**	**0.057**	**0.089**
OS3b	0.126	0.052	0.081	OS3b	0.103	0.042	0.066
O9	**0.090**	**0.037**	**0.058**	OS3a	0.098	0.040	0.063
O8	**0.083**	**0.034**	**0.053**	OS1d	0.085	0.035	0.055
Total fixed	**0.728**	**0.299**	**0.468**		**0.860**	**0.353**	**0.553**
Population	*	*	*		*	*	

	Ca1		Ca2		Ca3		Ca4
O11x3	0.238x3	O5x3	0.198x3	OS2a	0.561	OS3c	0.520
Cl1	0.449	O12x3	0.171x3	O15x3	0.228x3	O16x3	0.243x3
O10x3	0.151x3	Cl2	0.446	Cl3	0.517	Cl3	0.412
Cl2	0.417	Cl1	0.426	O13x3	0.143x3	O14x3	0.131x3
Total	2.033		1.979		2.191		2.054

Note: Parameters taken from Brese and O'Keeffe (1991). Bold = always occurring bonds; total fixed = bond valence sum, arising from always occurring bonds.
* Possible site population.

assignment of the vacancies at the split sites M4 and M4a as well as to the significant correlations between the parameters of the split sites ($r^2 > 0.69$) during the structural refinement. This interpretation is supported by noticing that U_{eq} of both M4 and M4a is more than 1.5 times that of the remaining sites (Table 4).

Thermal behavior

As a general remark it should be pointed out that the chemical composition of the crystals selected for the HT-XRPD investigation could differ from that of the crystal analyzed by EMPA and SREF.

At a first sight, the non-ambient X-ray powder diffraction data reveal no macroscopic modifications throughout the analyzed temperature range, apart from the expected effect of thermal expansion producing peak displacements and minor intensities modification. However, a close inspection of the data indicates that, at temperatures exceeding ca. 1000 K, the background increases. Moreover, at 1198 K a few weak extra reflections, apparently of a sodalite-like mineral, presumably haüyne $(Na,Ca,K)_{7-8}[Si_6Al_6O_{24}](SO_4)_2$, start to occur.

The background increase signals the occurrence of disordered material arising from the starting of the collapse of the afghanite structure.

A measurement carried out on the capillary slowly cooled-back to RT confirmed the occurrence of ca. 8 wt% of haüyne. The refined a cell parameter of 9.1135(4) Å is consistent with a K/Σcations ratio of 0.133 as derived from the regression equation $a = 9.071(2) + 0.032(2)\cdot$K/Σcations ratio of Ballirano and Maras (2005). This value is smaller than 0.159 determined from

EMPA in the studied afghanite sample. This behavior is similar to that reported for liottite, the ABABAC six-layer member of the sodalite-cancrinite supergroup (Ballirano 2012).

Insertion of haüyne in the refinements carried out on data collected at T above 1173 K provided a moderate improvement of the various Rietveld agreement indices. A weight fraction of 1.4 and 1.7 wt% of haüyne has been obtained at 1198 and 1223 K, respectively. According to such results, a significant fraction of haüyne is formed during the capillary cooling at the expenses of the coexisting disordered material.

The capillary was subsequently subjected to three heating/RT-cooling cycles at 1173 and 1198 K (twice), respectively. A comparison between the diffraction patterns collected at 1173 K during the heating process from 323 to 1223 K and that mea-

TABLE 8. Proposed populations of cation sites for afghanite at room T

Site	Mult.	Occupancy	No. e− refinement	%Na	%Ca	%K	Na	Ca	K	No. e− partititon
Ca1	2	1	40	0	100	0	0	2	0	40
Ca2	2	1	40	0	100	0	0	2	0	40
Ca3	2	1	40	0	100	0	0	2	0	40
Ca4	2	1	40	0	100	0	0	2	0	40
M1	6	0.791(4)	90.2(5)	50	0	50	3	0	3	90
M2	6	0.796(3)	90.8(3)	58	42	0	3.5	2.5	0	88.5
M3	6	0.573(3)	65.3(3)	100	0	0	6	0	0	66
M4	6	0.486(23)	55.4(26)	17	17	50	0.5	0.5	1.5	44
M4a		0.304(23)	34.7(26)	67	0	17	2	0	0.5	31.5
Total			496.4(63)				15.0	11.0	5.0	480.0
Chemical data			483.0				15.20	11.06	4.98	483.0

Notes: The M-site occupancies were obtained on the basis of the scattering power of K. Calculations were performed considering the M1, M2, and M3 sites as fully occupied, and a 5/6 occupation for M4+M4a.

sures after 2 days at 1173 K is reported in Figure 6. It is easy to observe the increased background and the occurrence of the extra peaks from haüyne.

Measurements at 1198 K did not provide significant modifications of the diffraction patterns as compared to those measured at 1173 K, indicating the relative sluggishness of the afghanite structure disruption and subsequent conversion to haüyne at those temperatures. Quantitative analyses, carried out by the Rietveld method, indicate a slow increase of the haüyne content that reaches approximately 12 wt% after the second heating cycle at 1198 K.

The repeated heating/RT-cooling cycles had as collateral effect the partial crystallization to tridymite of the SiO_2-glass capillary. This fact rendered the corresponding diffraction patterns significantly complex, due to the occurrence of the strong extra tridymite peaks. Therefore, it was impossible to obtain a correct structural model of afghanite under such conditions.

As far as the heating process from 323 to 1223 K is concerned, the dependence of unit-cell parameters and volume of afghanite from T has been investigated (Figs. 7a–7c). The corresponding relative expansion as a function of T is reported in Figure 8, the dependence of the isotropic displacement parameters from T in Figure 9, whereas that of the T-O-T angles is given in Figure 10. The results show that the unit-cell parameters increase with increasing T. Such an increase, however, is not linear due to occurrence of a discontinuity at 448 K, particularly evident for the c-parameter: up to 448 K, the c-parameter expands more than a (Figs. 7a and 7b). Above this discontinuity temperature (T_{d1}), the thermal expansion is reverted becoming greater for the a-parameter. A further discontinuity has been detected at 1073 K (T_{d2}) for the c-parameter, whereas its occurrence is less defined for the a-parameter and volume. The occurrence of a second discontinuity has been unequivocally observed for both cell parameters in liottite as well, at a comparable T of 1098 K (Ballirano 2012).

The volume thermal expansivity and the linear thermal expansion coefficients have been calculated following Fei (1995).
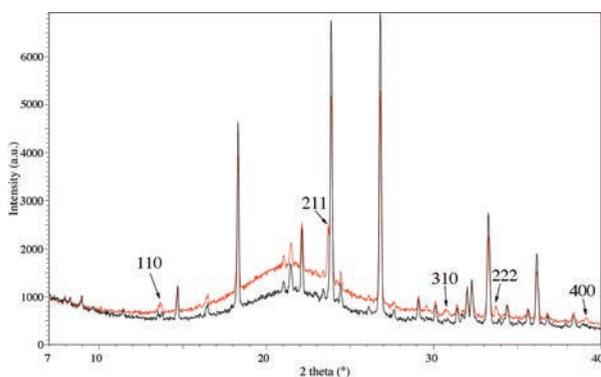

FIGURE 6. Comparison among the diffraction patterns collected during the heating process from 323 to 1223 K, at 1173 K, and that measured after 2 days at the same temperature. Comparison between the diffraction patterns collected at 1173 K during the heating process from 323 to 1223 K and that measured after 2 days at the same temperature. Relevant reflections of haüyne are indicated by arrows and indexed. (Color online.)
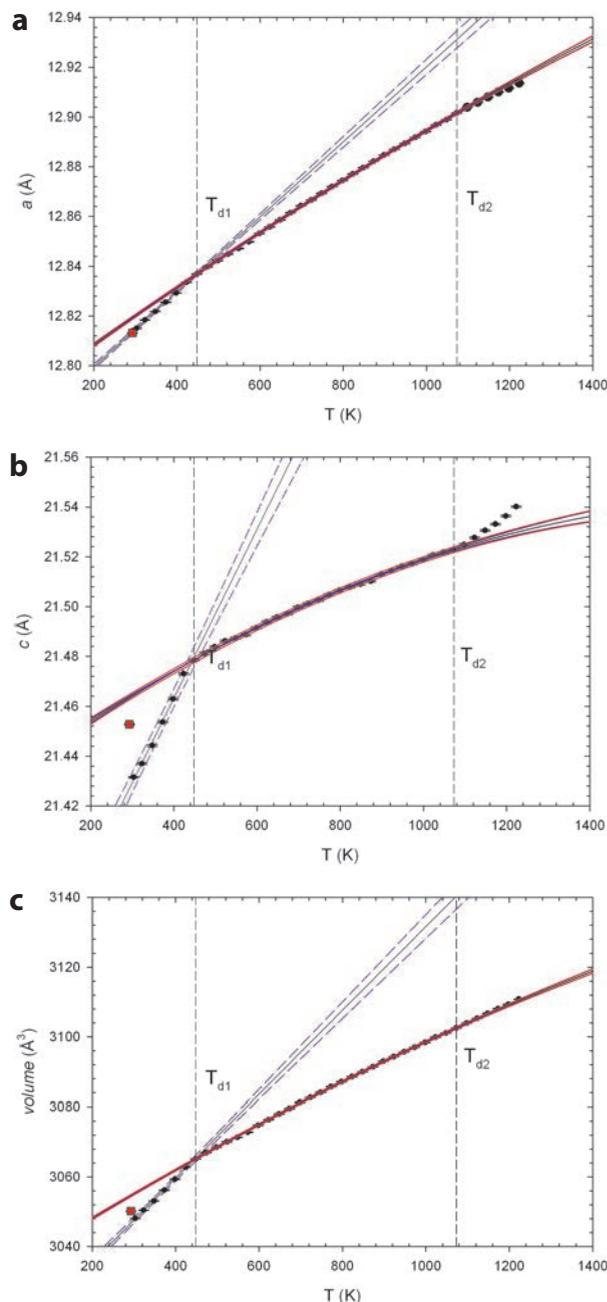

FIGURE 7. Evolution of cell parameters and volume of afghanite with temperature: (a) a cell parameter; (b) c cell parameter; (c) volume. The large square symbol refers to the cell of afghanite after cooling back to RT. Linear regression, confidence (95% level), and prediction intervals are reported for the first two thermal ranges ($323 < T < 448$ K and $448 < T < 1073$ K) as full, dotted, and short dash lines, respectively. (Color online.)

All the cell-volume data, for the three thermal ranges, were simultaneously fit to the equation $V(T) = V_{Tr} \exp[\int_{Tr}^{T} \alpha_V(T)dT]$ where V_{Tr} is the volume at reference temperature T_r and α_V is a polynomial of the form $\alpha_V = a_0 + a_1T + a_2T^{-2}$. Results of the fitting procedure, ignoring the T^{-2} term, are reported in Table 9. The corresponding mean thermal expansion coefficients $\overline{\alpha}_a$,
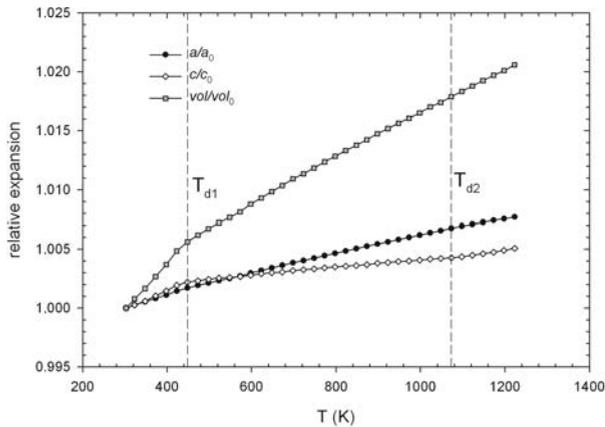
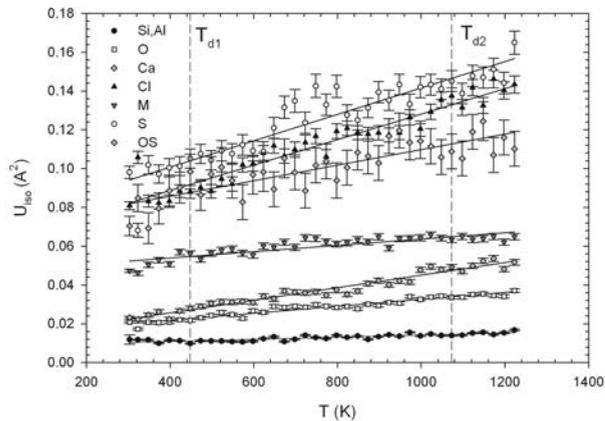**FIGURE 8.** Relative expansion of cell parameters and volume of afghanite.

FIGURE 9. Evolution of the isotropic displacement parameters of afghanite with temperature.

FIGURE 10. Evolution of the T-O-T angles of afghanite with temperature: (**a**) T-O$_{1-8}$-T; (**b**) T-O$_{9-16}$-T. (Color online.)

$\overline{\alpha_c}$, and $\overline{\alpha_V}$ were calculated by truncating the exponential series of $\exp[a_0(T - T_r)]$ at its second order. The T-dependent a_1 coefficients are generally small indicating independence from temperature. In fact, fitting of the data to the expression $V(T) = V_{Tr}[1 + \alpha(T - T_r)]$ provided determination coefficients R^2 only marginally worse than those obtained from fitting the data to the equation $V(T) = V_{Tr} \exp[\int_{Tr}^{t} \alpha_V(T)dT]$, the only exception being the c-parameter in the $448 < T < 1223$ K thermal range. There is a general regular decrease of the mean linear and volume thermal expansion coefficients as T increases with the only exception of the c-parameter above T_{d2} whose $\overline{\alpha_c}$ value increase. It should be noticed that Bonaccorsi et al. (1995) reported the occurrence of a discontinuity in the expansion of the c-parameter, similar to that occurring in afghanite. Besides, the temperature at which the discontinuity occurs in the present afghanite (448 K) is similar to those reported by Bonaccorsi et al. (1995) for microsommite and davyne from Zabargad: 433 and 473 K, respectively. Such a discontinuity has been attributed, in the case of microsommite, to the tilting of the tetrahedra connected along [001] and the occurrence of a purely displacive phase transition from space group $P6_3$ to 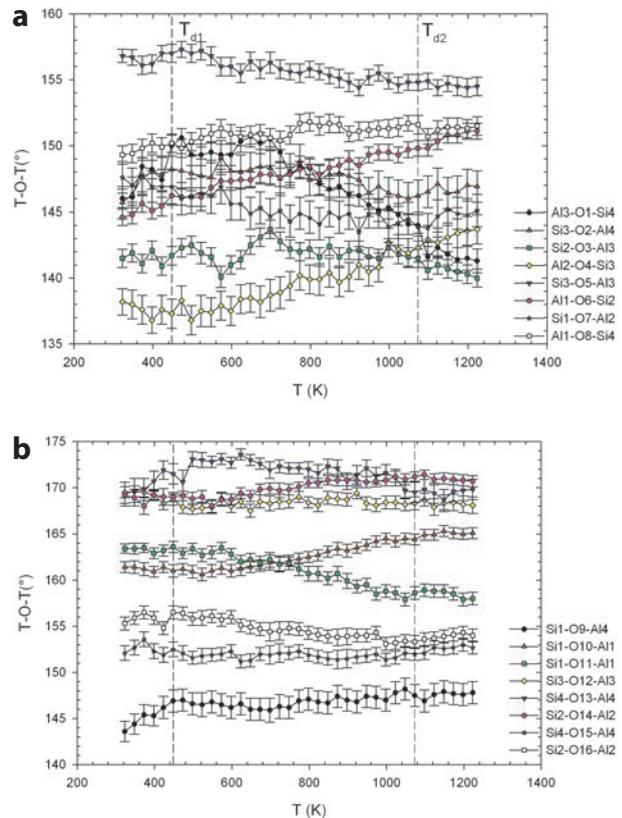$P6_3/m$. This cannot be the case of afghanite as an increase in symmetry is incompatible with a fully ordering of Si and Al among the different tetrahedral sites building up the framework that has been proved to be maintained throughout the investigated thermal range (see below). The reported discontinuity consistently marks a significant reduction of the mean thermal expansion coefficients. In the case of these Cl- and SO$_4$-bearing minerals, the a cell parameter has a larger thermal expansion with respect to the c cell parameter above the discontinuity, as indicated by values of $\overline{\alpha_a}$ in the 6.5–15.5 K^{-1} range and of $\overline{\alpha_c}$ in the 1.5–3.6 K^{-1} range (Ballirano 2012). No direct comparison can be performed with thermal expansion data of cancrinite (Hassan et al. 2006) because the thermal behavior depends on dehydration and significant extraframework cation rearrangement.
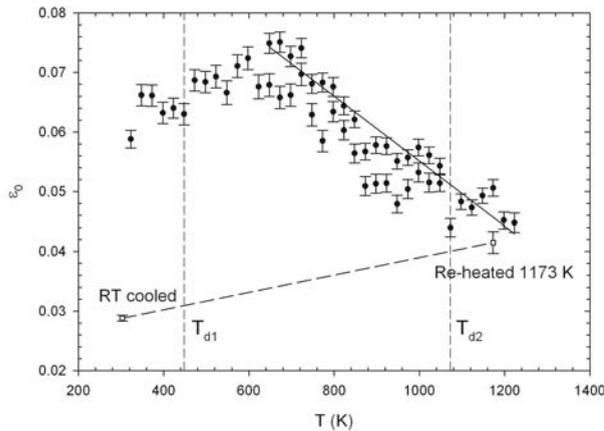
Isotropic displacement parameters increase linearly with increasing T (Fig. 9) and scale reasonably well with those reported at 943 K for the microsommite framework. On the contrary, extraframework cations and anions show larger isotropic displacement parameters as compared to those of microsommite, indicating the development of further positional cation disorder and a more complex arrangements for the sulfate groups as temperature increases. The exception to this trend is shown by the Ca atoms, which are perfectly ordered at RT and show isotropic displacement parameters consistent with those observed at HT for microsommite.

As far as the framework modifications are concerned, tetra-

TABLE 9. Linear and volume thermal expansion coefficients a_0 and a_1 and mean linear and volume thermal expansion coefficients $\overline{\alpha_a}, \overline{\alpha_c}$, and $\overline{\alpha_v}$ of afghanite

		323 K < T < 448 K T_r = 323 K	448 K < T < 1073 K T_r = 448 K	1073 K < T < 1223 K T_r = 1073 K
a-parameter	R^2	0.9823/*0.9822*	0.9998/*0.9993*	0.9991/*0.9952*
	a_0 (× 10^{-6})	13.1(18)	8.70(5)	7.07(16)
	a_1 (× 10^{-8})	1(1)	−0.101(9)	−0.60(13)
	a_{T_r}	12.81673(13)	12.83684(4)	12.90157(11)
	$\overline{\alpha_a}$(× 10^{-6})	12.9(4)	8.22(3)	6.35(9)
c-parameter	R^2	0.9614/*0.9614*	0.9987/*0.9871*	0.9987/*0.9845*
	a_0 (× 10^{-6})	18(4)	4.22(5)	3.87(18)
	a_1 (× 10^{-8})	1(3)	−0.147(10)	0.95(14)
	c_{T_r}	21.4328(4)	21.4785(8)	21.5229(3)
	$\overline{\alpha_c}$ (× 10^{-6})	17.9(9)	3.52(4)	5.02(14)
V	R^2	0.9751/*0.9751*	0.9999/*0.9977*	0.9995/*0.9994*
	a_0 (× 10^{-6})	44(7)	21.61(10)	18.1(4)
	a_1 (× 10^{-8})	1(1)	−0.34(2)	−0.3(3)
	V_{T_r}	3049.04(7)	3065.15(7)	3102.53(6)
	$\overline{\alpha_v}$ (× 10^{-6})	43.7(18)	19.68(8)	17.74(9)

Notes: Linear and volume thermal expansion coefficients were obtained by fitting the data to the expression $\alpha_v(T) = a_0 + a_1T$. a_{T_r}, c_{T_r}, and V_{T_r} are the a-parameter, c-parameter, and volume at reference temperature T_r. R^2 = determination coefficient for the linear and volume thermal expansion coefficients. Values in italic refer to the determination coefficient of the mean linear and volume thermal expansion coefficient.

FIGURE 11. Dependence of ε_0 microstrain on temperature.

FIGURE 12. Dependence on temperature of the vertical distances between pairs of T cations (Si-Si and Al-Al) pertaining to the bases of the Cl3-centered cancrinite cage. The average value has been used as a measure of the cage height.

hedral bond distances are quite constant throughout the whole analyzed thermal range (1.596 < Si-O < 1.635 Å; 1.705 < Al-O < 1.765 Å), differently from the findings of Hassan et al. (2006) for cancrinite (1.482 < Si-O < 1.750 Å; 1.564 < Al-O < 1.815 Å) from synchrotron radiation X-ray powder diffraction data. This is possibly due, as pointed out by Ballirano et al. (2011b, 2011c) in the case of calcite and nitratine, by the use of an extended $\sin\theta/\lambda$ range as compared to Hassan et al. (2006).

T-O-T dependence from T shows very interesting features (Fig. 10). As a general comment, the regularity of the behavior of many T-O-T angles as a function of T is remarkable, confirming the overall stability of the refinements. In detail, Al2-O4-Si3, Al1-O6-Si2, Al1-O8-Si4, and Si2-O14-Al2 increase with increasing T; Si3-O5-Al3, Si1-O7-Al2, and Si1-O11-Al1 decrease with increasing T; Si3-O2-Al4, Si2-O3-Al3, Si1-O9-Al4, Si1-O10-Al1, Si3-O12-Al3, Si4-O13-Al4, Si4-O15-Al4, and Si2-O16-Al2 are substantially independent from T. In the case of Al3-O1-Si4 the angle increases to a maximum value,

at a temperature exceeding T_{d1}, and subsequently it decreases.

The dependence of microstrain ε_0 (Ballirano and Sadun 2009) with temperature shows that up to 700 K, ε_0 increases to a maximum value of ca. 0.075 but above this temperature it decreases with increasing temperature up to ca. 0.04 (Fig. 11). However, cooling the sample to RT led to a release of the strain to 0.0284(5). This process is coupled with a significant expansion of the c-parameter as compared to the starting RT data (Fig. 7b). Moreover, upon reheating at 1173 K, the microstrain increases back to approximately the same value calculated at the corresponding temperature during the first heating process. Repeated heating/cooling cycles did not modify the ε_0 values both at RT and at HT. Therefore, the strain release occurs prevalently during the first heating/cooling cycle.

It is worth noting that ε_0 reaches the largest value approximately in correspondence of the maximum expansion of the Al3-O1-Si4 angle. As this angle is one of those governing the expansion of the Cl3-centered cancrinite cage, its height dependence with T follows essentially the same behavior of the Al3-O1-Si4 angle attaining a maximum value of 5.361 Å at 748 K (Fig. 12). Therefore, it seems reasonable to relate the behavior of microstrain with the one of the ε cage. The fact that the strain release is accompanied by a c-parameter expansion should be mostly due to the expansion of that cage after the heating/cooling cycle. In fact, the normalized c-parameter c_n [$c_n = 2c/(N)$; N = number of layers] (Sapozhnikov 2004) of the cooled back afghanite takes the value of ca. 5.364 Å, corresponding to that of a fully expanded Cl-bearing cancrinite cage. However, despite the lower quality of the structural data for the RT cooled back data collection compared to the non-ambient ones, due to the presence of approximately 8 wt% of haüyne mixed with afghanite, the cage height has been found to be of 5.353 Å confirming a significant expansion with respect to the untreated sample.

REFERENCES CITED

Ballirano, P. (1994) Crystal chemical investigation of cancrinite-like minerals, 167 p. Ph.D. thesis, Sapienza Università di Roma (in Italian).

——— (2003) Effects of the choice of different ionization level for scattering curves and correction for small preferred orientation in Rietveld refinement: The $MgAl_2O_4$ test case. Journal of Applied Crystallography, 36, 1056–1061.

——— (2011a) Thermal behavior of natrite Na_2CO_3 in the 303–1013 K thermal range. Phase Transitions, 84, 357–374.

——— (2011b) Laboratory parallel beam transmission X-ray powder diffraction investigation of the thermal behavior of calcite: comparison with X-ray single-crystal and synchrotron powder diffraction data. Periodico di Mineralalogia, 80, 123–134.

——— (2011c) Laboratory parallel beam transmission X-ray powder diffraction investigation of the thermal behavior of nitratine $NaNO_3$: Spontaneous stress and structure evolution. Physics and Chemistry of Minerals, 38, 531–541.

——— (2012) The thermal behaviour of liottite. Physics and Chemistry of Minerals, 39, 115–121.

Ballirano, P. and Maras, A. (2005) Crystal chemical and structural characterization of an unusual CO_3-bearing sodalite-group mineral. European Journal of Mineralogy, 17, 805–812.

Ballirano, P. and Melis, E. (2007) Thermal behaviour of β-anhydrite $CaSO_4$ to 1,263 K. Physics and Chemistry of Minerals, 34, 699–704.

Ballirano, P. and Sadun, C. (2009) Thermal behavior of trehalose dihydrate (T_h) and b-anhydrous trehalose (T_b) by in-situ laboratory parallel-beam X-ray powder diffraction. Structural Chemistry, 20, 815–823.

Ballirano, P., Maras, A., Caminiti, R., and Sadun, C. (1995) Carbonate-cancrinite: in situ real time thermal processes studied by means of energy-dispersive X-ray powder diffractometry. Powder Diffraction, 10, 173–177.

Ballirano, P., Maras, A., and Buseck, P.R. (1996a) Crystal chemistry and IR spectroscopy of Cl- and SO_4-bearing cancrinite-like minerals. American Mineralogist, 81, 1003–1012.

Ballirano, P., Merlino, S., Bonaccorsi, E., and Maras, A. (1996b) The crystal structure of liottite, a six-layer member of the cancrinite group. Canadian Mineralogist, 34, 1021–1030.

Ballirano, P., Bonaccorsi, E., Maras, A., and Merlino, S. (1997) Crystal structure of afghanite, the eight-layer member of the cancrinite-group: Evidence for Si,Al long range ordering. European Journal of Mineralogy, 9, 21–30.

Bariand, P., Cesbron, F., and Giraud, R. (1968) Une nouvelle espèce minérale: l'afghanite de Sar-e-Sang, Badakhshan, Afghanistan. Comparaison avec les minéraux du groupe de la cancrinite. Bulletin de la Société Française de Minéralogie et de Cristallographie, 91, 34–42.

Bonaccorsi, E. and Merlino, S. (2005) Modular microporous minerals: cancrinite-davyne group and C-S-H phases. Revue of Mineralogy and Geochemistry, 57, 241–290.

Bonaccorsi, E., Comodi, P., and Merlino, S. (1995) Thermal behaviour of davyne-group minerals. Physics and Chemistry of Minerals, 22, 367–374.

Bonaccorsi, E., Ballirano, P., and Cámara, F. (2012) The crystal structure of sacrofanite, the 74Å phase of the cancrinite-sodalite supergroup. Microporous and Mesoporous Materials, 147, 318–326.

Brese, N.E. and O'Keeffe, M.O. (1991) Bond-valence parameters for solids. Acta Cristallographica, B47, 192–197.

Bruker AXS (2009) Topas V4.2: General profile and structure analysis software for powder diffraction data. Bruker AXS, Karlsruhe, Germany.

Cheary, R.W. and Coelho, A. (1992) A fundamental parameters approach to X-ray line-profile fitting. Journal of Applied Crystallography, 25, 109–121.

Chukanov, N.V., Rastsvetaeva, R.K., Pekov, I.V., and Zadov, A.E. (2007) Alloriite,

$Na_5K_{1.5}Ca(Si_6Al_6O_{24})(SO_4)(OH)_{0.5}·H_2O$, a new mineral species of the cancrinite group. Geology of Ore Deposits, 49, 752–757.

Fei, Y. (1995) Thermal expansion. In J.A. Ahrens, Ed., A Handbook of Physical Constants, Mineral Physics and Crystallography. AGU Reference Shelf 2, 29–44.

Finger, L.W., Cox, D.E., and Jephcoat, A.P. (1994) A correction for powder diffraction peak asymmetry due to axial divergence. Journal of Applied Crystallography, 27, 892–900.

Hassan, I. (1996a) The thermal behaviour of cancrinite. Canadian Mineralogist, 34, 893–900.

——— (1996b) Thermal expansion of cancrinite. Mineralogical Magazine, 60, 949–956.

Hassan, I., Antao, S.M., and Parise, J.B. (2006) Cancrinite: Crystal structure, phase transitions, and dehydration behaviour with temperature. American Mineralogist, 91, 1117–1124.

Ivanov, V.G. and Sapozhnikov, A.N. (1975) First finding of afghanite in U.S.S.R. Zapiski Vsesoyuznogo Mineralogicheskogo Obshchestva, 104, 3328–3331 (in Russian).

Larson, A.C. and Von Dreele, R.B. (2000) General Structure Analysis System (GSAS). Los Alamos National Laboratory Report LAUR 86-748.

McCusker, L.B., Liebau, F., and Engelhardt, G. (2001) Nomenclature of structural and compositional characteristics of ordered microporous and mesoporous materials with inorganic hosts. Pure and Applied Chemistry, 73, 381–394.

Merlino, S. and Mellini, M. (1976) Crystal structure of cancrinite-like minerals. Zeolite '76, Proceedings of International Conference on the occurrence, properties, and utilization of natural zeolites (Tucson). Program and Abstracts, 47.

Parodi, G.C., Ballirano, P., and Maras, A. (1996) Afghanite from Mount Vesuvius: a rediscovery. Mineralogical Record, 27, 109–114.

Pobedimskaya, E.A., Rastsvetaeva, R.K., Terent'eva, L.E., and Sapozhnikov, A.N. (1991) Crystal structure of afghanite. Doklady Akademii Nauk S.S.S.R., 320, 882–886 (in Russian).

Rastsvetaeva, R.K., Ivanova, A.G., Chukanov, N.V., and Verin, I.A. (2007) Crystal structure of alloriite. Doklady Earth Sciences, 415, 815–819.

Sapozhnikov, A.N. (2004) Influence of the chemical composition on the framework configuration of cancrinite-like minerals. Micro- and Mesoporous Mineral Phases (Accad Lincei, Roma) Volume Abstracts 290–293.

Sheldrick, G.M. (2008) A short history of SHELX. Acta Crystallographica, A64, 112–122.

Thompson, P., Cox, D.E., and Hastings, J.B. (1987) Rietveld refinement of Debye-Scherrer synchrotron X-ray data from Al_2O_3. Journal of Applied Crystallography, 20, 79–83.

Toby, B.H. (2001) EXPGUI, a graphical user interface for GSAS. Journal of Applied Crystallography, 34, 210–213.

Von Dreele, R.B. (1997) Quantitative texture analysis by Rietveld refinement. Journal of Applied Crystallography, 30, 517–525.

Young, R.A. (1993) Introduction to the Rietveld method. In R.A. Young, Ed., The Rietveld Method, p. 1–38. Oxford, U.K.